Phasor and Simplified Average Models of Two-Stage Single-Phase PV System

Maryam Mahmoudi Koutenaei
Student Member, IEEE
Florida International University
Miami, FL, USA
mmahm024@fiu.edu

Thanh Thai Nguyen
Member, IEEE
Clarkson University
Potsdam, NY, USA
tnguyen@clarkson.edu

Tuyen Vu
Member, IEEE
Clarkson University
Potsdam, NY, USA
tvu@clarkson.edu

Sumit Paudyal
Member, IEEE
Florida International University
Miami, FL, USA
spaudyal@fiu.edu

***Abstract*—The computational challenge in solving dynamic models of power distribution grids increases with high penetration of distributed photovoltaic (PV) systems. IEEE-1547 requires smart PV inverters to provide dynamic volt-var and volt-watt support functions, which motivates solving dynamics of large distribution grids with multiple distributed PVs. The existing dynamic models of PV systems are overly detailed and computationally intractable for solving distribution grid dynamics with a large number of distributed PVs. In this work, a simplified average model and a phasor-based model of a two-stage single-phase smart PV system are developed and compared with the existing average and detailed models in literature. The results show remarkably fast performance from the proposed phasor-based and simplified average models of PVs, while sufficiently capturing necessary volt-var and volt-watt dynamics.**

***Index Terms*—phasor model, simplified average model, smart inverters, volt-var, volt-watt**

I. Introduction

The number of residential photovoltaic (PV) systems in distribution grids is increasing significantly. To study the impact of the high penetration of residential PV systems in distribution grid, development of a fast and accurate model of the PV systems becomes absolutely necessary. The detailed switching model of the PV system provides every detail of the PV system and its control development, which is highly complex and computationally burdensome for network level studies. Study [1] clearly shows that neither the switching model nor the average model are computationally tractable for large distribution feeders with multiple distributed inverters. A simplified model of the PV system was developed in [2] which removes the DC-side dynamics related to PV array, Maximum Power Point Tracking (MPPT), and DC-link. However, the proposed model fails to reflect the dynamics caused by irradiance change, temperature variation, and DC-link voltage fluctuation. Another simplified model of the PV system introduced in [3] for time-domain simulation eliminates fast dynamics related to MPPT controller, inner current control loop, DC-side and AC-side switching ripple filters. In the same work, the phasor model was also introduced, which has lower solve time. In [3], PI controllers are employed to track the sinusoidal current reference. However, a PI controller has steady-state error when tracking a sinusoidal reference signal [4]. Moreover, this work [3] is unable to provide reactive power control as well as voltage support using volt-var and volt-watt functions. In this paper, a phasor-based model of two-stage single-phase smart PV system is proposed. In this modeling procedure, the major efforts are put to resolve the aforementioned issues associated with the existing models. To achieve this, first, a simplified average model of PV system is developed to achieve controllable DC values for PI current controllers. Second, in the proposed model, smart features including volt-var and volt-watt functions (as per IEEE 1547) are considered. Moreover, the PV side controller is enabled to operate either in the MPPT or active power curtailment mode. The later mode always makes PV to operate under the PV's inverter rated power. Additionally, in the simplification stage the inner current loops and DC-side LC filters are removed. The LCL filter is kept as it captures the dynamical interaction between the inverter and the grid [1].

This work is supported by National Science Foundation (NSF) grant ECCS-2001732.

This paper is divided into five sections. Section II describes the smart PV system power circuit and control configuration. An overview of the existing models (detailed and average models) of the PV systems are given in section III. The proposed simplified average and phasor models are described in detail in section IV. Section V validates the proposed models through several case studies. The conclusions are drawn in section VI.

II. Power circuit and control configuration of the smart PV system

Typical configuration of two-stage single-phase smart PV system is shown in Fig. 1 [5]. Power circuit consists of a PV array model, LC harmonic filter, boost converter, Dc link capacitor, full-bridge inverter and LCL filter. Active and reactive power support of the grid are performed through PV-side and Grid-side controllers.

A. Photovoltaic Array Model

The PV array in Fig. 1 is modeled through the single-diode PV model. The current-voltage (I_{PV} - V_{PV}) relationship of a

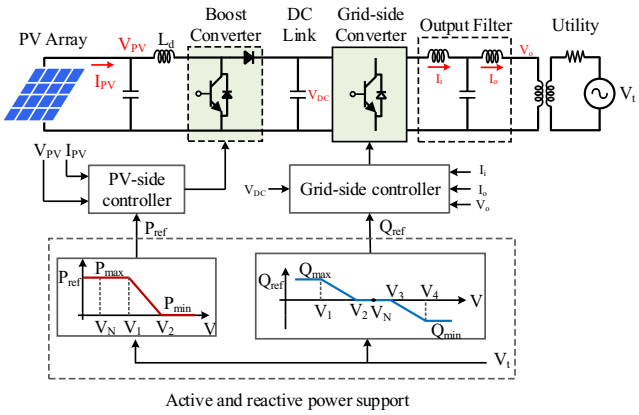

Fig. 1. Typical configuration and control of PV system [5], with active and reactive power support function as per the IEEE-1547.

single PV module is presented as [6],

$$I_{PV} = I_{ph} - I_0\left[exp\left(\frac{V_{PV} + I_{PV}R_s}{N_c V_T}\right) - 1\right] - \frac{V_{PV} + I_{PV}}{R_{sh}} \tag{1}$$

where N_c is the number of series cells in the module; R_s and R_{sh} are the series resistance and shunt resistance; I_{ph} is the photo current; I_0 is the diode saturation current; V_T is the thermal voltage expressed through $V_T = kAT/q$, where k is the Boltzmann's constant; q is the electron charge and A is the diode ideality factor which is a small number close to 1. The parameters I_{ph}, I_0, R_{sh}, and R_s are estimated for standard test condition (STC) which are given in Table. I. Then, the only parameters which are considered to change with irradiance and temperature are I_0 and I_{ph}, and are updated through (2) and (3) respectively [6] as,

$$I_0 = I_{0,STC}\left[\frac{T}{T_{STC}}\right]^3 exp\left(\frac{qE_g}{Ak}\left(\frac{1}{T_{STC}} - \frac{1}{T}\right)\right) \tag{2}$$

$$I_{ph} = (I_{ph,STC} + k_i\Delta T)G \tag{3}$$

where $T_{STC} = 273.15k$ is the temperature at STC; $E_g = 1.1e.v.$ is the silicon bandgap energy; K_i is the short circuit current temperature coefficient and G is the irradiance ratio.

B. PV-side and Grid-side controllers

The PV-side controller regulates the generated power of the PV by controlling the duty cycle of the boost converter. It operates either on Maximum Power Point Tracking (MPPT) or Constant Power Generation (CPG) mode. CPG mode curtails the PV power to P_{ref} which is obtained either by the volt-watt droop characteristic (active power support function) or by (4) to meet the inverter apparent power constraint S_{rated} during volt-var mode (reactive power support function). The perturb and observe algorithm is used in this work for both the MPPT and CPG modes [7].

$$P_{ref} = \sqrt{S_{rated}^2 - Q_{ref}^2} \tag{4}$$

The main function of the grid-side controller is to regulate the DC-link voltage and reactive power output of the full-bridge inverter. The default control mode of the PV system is the unity power factor or MPPT mode. The others are volt-watt (active power support function) and volt-var (reactive power support function) control modes, as shown in Fig. 1. The reactive power reference Q_{ref} in the volt-var mode and the maximum limit of the PV power P_{ref} in the volt-watt mode are functions of the smart inverter output voltage. The droop settings follow the IEEE-1547 default droop settings which are given in Table II.

III. Existing Models of the PV System

The most-commonly used models of the PV systems include detailed and average models. The difference between those models are the converters modelling and control; however, the active and reactive power support function remain the same. The detailed model can represent the accurate behavior of the PV systems including harmonics but it is computationally inefficient. The average model can provide similar behavior and accurate dynamic response when compared to the detailed model.

A. Detailed Model

The detailed model uses the switching devices for the boost converter and the full-ridge inverter [1]. The PV-side and grid-side control diagram of the detailed switching converter is shown in Fig. 2. The grid-side controller is responsible for the regulation of DC-link voltage and managing output reactive power. The DC-link voltage and reactive power controllers generate dq current references for the inner current control loop. The dq components of single-phase current and voltage are obtained by using (5), in which the phase angle (ωt) of utility grid voltage is given by the single-phase phase-locked loop (PLL), as shown in Fig. 2.

$$\begin{bmatrix} f_d \\ f_q \end{bmatrix} = \begin{bmatrix} \cos(\omega t) & \sin(\omega t) \\ -\sin(\omega t) & \cos(\omega t) \end{bmatrix} \begin{bmatrix} f_\alpha \\ f_\beta \end{bmatrix}. \tag{5}$$

where f_α and f_β are the real and imaginary parts of the single phase signal, in which the real part f_α is the original signal and the imaginary part f_β is obtained by shifting the original signal by 90°. The fixed 90° phase shift between real and imaginary parts is constructed by a quarter-cycle delay [8]. The proportional-integral (PI) regulators are used to compensate for the errors in the controlled signals. The duty cycle is generated by the inner current loop to regulate the inverter current to follow the references. The pulse width modulation (PWM) uses the duty cycle as the input to provide the switching signals for the converters.

B. Average Model

The first step of simplification of the detailed model is replacing the switching devices of (the boost converter and full-bridge inverter) in the detailed model with their equivalent average models. More details about equivalent average models of the switching devices are provided in [1]. The control diagram of the average model is the same as the detailed model except for the absence of PWM modules. Thus, this model maintains all dynamics of the detailed model except for the fast dynamics related to switching devices and PWM modules.

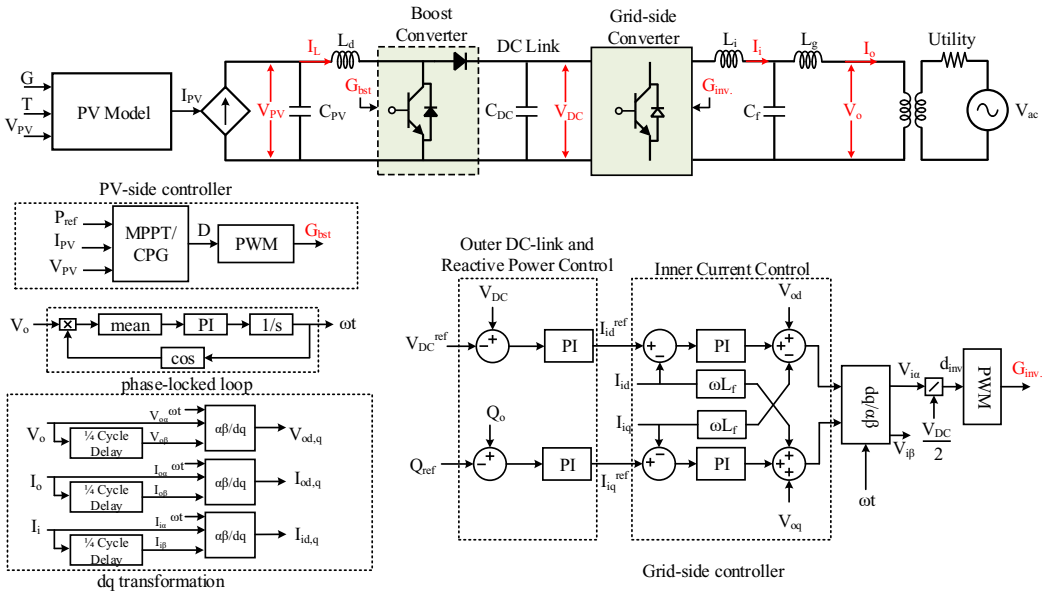

Fig. 2. Detailed model of smart inverter.

IV. Proposed Models

A. Simplified Average Model

Although the average model of the PV system is much faster than the detailed model, it is still computationally burdensome for modeling a large number of the residential smart PV systems. The high-frequency dynamics of the average model are related to the inner current control loops and harmonic filters [9]. Therefore, to obtain a simplified average model (as shown in Fig. 3) the inner current control loops and harmonic filters are removed to eliminate fast dynamics; whereas the outer voltage loop, DC-link capacitor, and LCL filter are retained. This helps maintain the dynamic interaction between the grid-side converter and PV-side converter, and the dynamic interaction between the grid-side converter and the grid, respectively. Referring to Fig. 3, in the simplified average model, $V_{PV} = (1 - D)V_{DC}$ (D is the duty cycle obtained by MPPT/CPG). The inverter is modeled as a controlled current source whose current reference is obtained via DC-link voltage and reactive power control loops. Moreover, the DC-link is modeled to represent the interaction between the inverter output active power P_o and the power generated by the PV P_{PV}, as expressed in (6).

$$C_{dc}\frac{dV_{DC}}{dt} = \frac{P_o - P_{PV}}{V_{DC}} \tag{6}$$

B. Phasor-based Model

Even though, the simplified average model derived in the previous section has an acceptable performance in time-domain simulation, it is not suitable for fast phasor-based simulation of large distribution grids. Therefore, the phasor-based model of the smart PV system, which is shown in Fig. 4, is proposed in this section. Referring to the Fig. 4, the phasors of the current and voltage signals of the proposed model are denoted by the inverter output voltage $|V_{om}|\angle\theta_{vo}$ and output current $|I_{om}|\angle\theta_{io}$, respectively. In the phasor domain, the signals type are complex at the grid frequency and the phase-locked loop (PLL) block is not required hence removed from model. The dq components of the output voltage are set as $V_{oq} = 0$ and $V_{od} = |V_{om}|$. Therefore, the dq components of the phasor signal $f = |f_m|\angle\theta_f$ are given by (7) and (8), and the phasor representation of the f_d and f_q is obtained by (9) to (11).

$$f_d = |f_m|\cos\left(\theta_f - \theta_{vo}\right) \tag{7}$$

$$f_q = |f_m|\sin\left(\theta_f - \theta_{vo}\right) \tag{8}$$

$$|f_m| = \sqrt{f_d^2 + f_q^2} \tag{9}$$

$$\theta_f = \arctan\left(\frac{f_q}{f_d}\right) + \theta_{vo} \tag{10}$$

$$f = |f_m|\angle\theta_f \tag{11}$$

V. Results and Discussion

The efficiency and accuracy of the proposed simplified average and phasor-based models of a 5 kW two-stage single-phase PV system are evaluated in this section. The specifications of the under-test system are given in Table I. The detailed model is employed as a benchmark. Moreover, the average model is also compared and assessed.

A. Solar Irradiation Fluctuation

Fig. 5(a) shows the solar irradiation variation which goes down by two step changes from 1 p.u. to 0.5 p.u and then goes back to 1 p.u. Fig. 5(b) presents the dynamic response of the output active power of four discussed models. In entire duration of simulation, the proposed simplified average and phasor-based model have shown higher accuracy; the maximum difference of their active power with the ones from the detailed and average models are 0.95% and 0.34%, respectively. It is worth mentioning that the reason for lowest active power of detailed model is switching and resistive losses, which are ignored in other models.

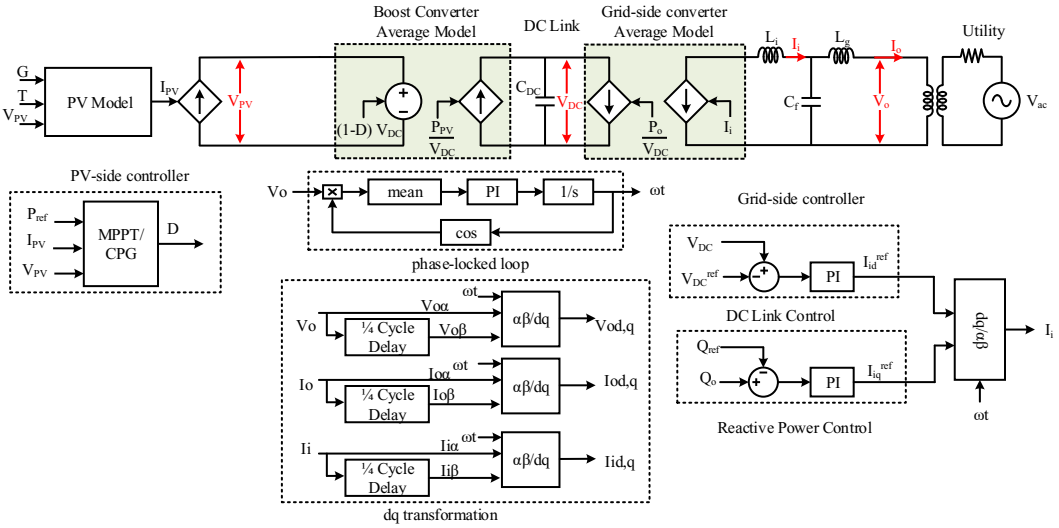

Fig. 3. Simplified average model of smart inverter.

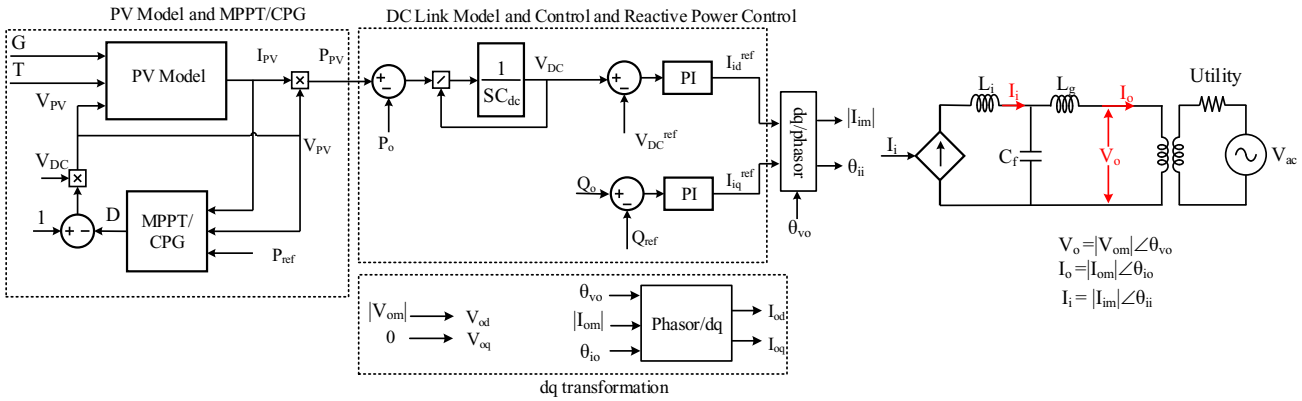

Fig. 4. The proposed phasor-based model.

B. Low Voltage Ride-Through (LVRT) Performance and Volt-Var function

According to IEEE 1547 [10], LVRT capability means that a smart inverter continues injecting current even when the voltage drops into the low voltage ride-through operating region (0.5-0.88 p.u). Fig. 6 depicts the PV system performance during low voltage event and normal condition. The irradiance is at maximum level, the grid voltage changes according to Fig. 6(a) and the inverter is set to vol-var function mode. The volt-var droop settings are given in Table II. As shown in Fig. 6(b), the smart inverter is injecting reactive power when the voltage sags (1-2.5 s) and is absorbing reactive power when the voltage swells (3-4 s) which means that the inverter is able to provide dynamic voltage support to the grid during LVRT and normal operation. Moreover, the CPG mode of the PV-side controller is enabled during reactive power injection and absorption as shown in Fig. 6(c). Not only does this case study verifies the proper LVRT performance and volt-var functionality of the designed smart PV inverter, it also demonstrates that the proposed simplified and phasor models closely match the detailed and average models.

C. Dynamic over-voltage support using volt-watt function

The smart PV system's capability of the dynamic over-voltage support using volt-watt function is evaluated in this scenario. The irradiance is at the maximum level and the inverter is set to vol-watt function mode (the reactive power reference is set to zero). The volt-watt droop characteristic and settings are given in Fig. 1 and Table II, respectively. As it can be seen from Fig. 7(a) and (b), during 0.5-1.5 s, the bus voltage is 1 p.u. Thus, the PV system works on the MPPT mode. However, during 1-3 s, since the bus voltage increases from 1 p.u. to 1.09 p.u. by four step changes, the active power is curtailed to the P_{ref} values obtained by the volt-watt droop characteristic to decrease the smart PV inverter output active power. The active power plots of the four described models in Fig. 7(b) show that the designed smart PV system successfully supports the grid voltage during over-voltage events by reducing its output active power to an amount obtained by volt-watt droop characteristics.

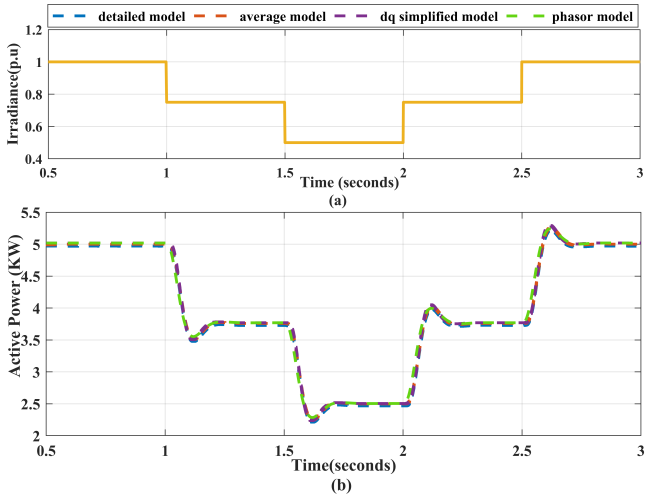

Fig. 5. Case study A. Solar irradiation fluctuation. (a) Irradiance profile, (b) Output active power.

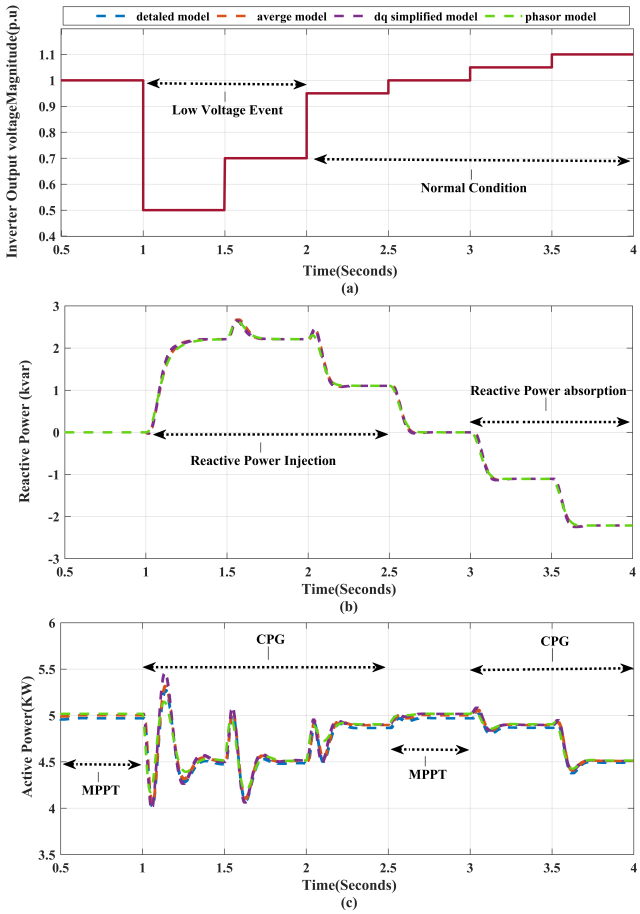

Fig. 6. Case study B. LVRT Performance. (a) Output voltage (b) Output reactive power.

D. Computational Performance

The execution time of LVRT case study of the all presented models for a 4-second simulation is compared in Table III. The simulation is performed in MTLAB/Simulink R2019b using a PC with 2.9 GHZ CPU and 16 GB RAM. As summarized in

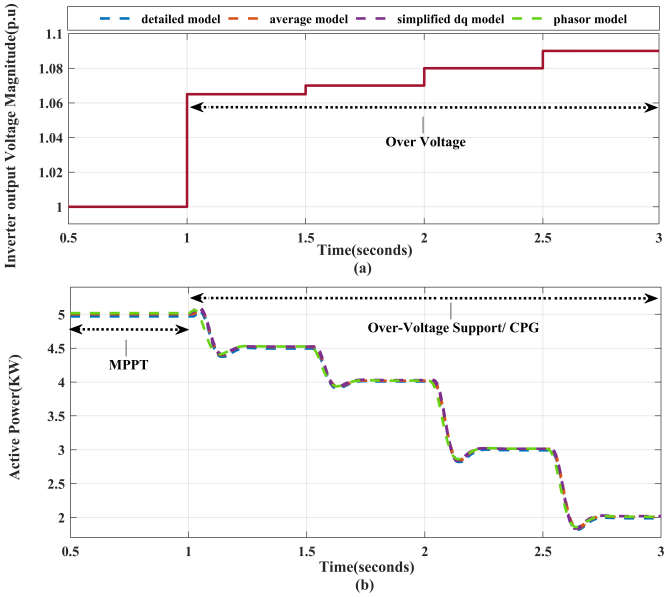

Fig. 7. Case study C.volt-watt function . (a) Inverter output Voltage magnitude, (b) output active power.

Table III, although the developed simplified average model is much faster than the average and detailed models, the proposed phasor model is the fastest model which is more than an order of magnitude faster than the average model and more than two orders of magnitude faster than the detailed model.

VI. Conclusion

In this paper, the simplified average and phasor models of a two-stage single-phase PV system are developed in compliance with the IEEE-1547 standard. Therefore, they incorporate vol/var and volt/watt control functions, and LVRT capability to fulfill the grid-code requirements. The comparison study with the existing PV models (detailed and average models) proved the efficiency and accuracy of the presented models. It is worth mentioning that the simplified average model is computationally efficient model for time-domain simulations, and the phasor model is computationally efficient and suitable for phasor-based simulations.

References

[1] E. I. Batzelis, G. Anagnostou, I. R. Cole, T. R. Betts, and B. C. Pal, "A state-space dynamic model for photovoltaic systems with full ancillary services support," *IEEE Transactions on Sustainable Energy*, vol. 10, no. 3, pp. 1399–1409, 2019.

[2] M. Patsalides, V. Efthymiou, A. Stavrou, and G. E. Georghiou, "A generic transient PV system model for power quality studies," *Renewable Energy*, vol. 89, pp. 526–542, 2016.

[3] X. Mao and R. Ayyanar, "Average and phasor models of single phase PV generators for analysis and simulation of large power distribution systems," in *Proc. Twenty-Fourth Annual IEEE Applied Power Electronics Conference and Exposition*, 2009, pp. 1964–1970.

[4] A. Kuperman, "Proportional-resonant current controllers design based on desired transient performance," *IEEE Transactions on Power Electronics*, vol. 30, no. 10, pp. 5341–5345, 2015.

[5] P. K. Pardhi, S. K. Sharma, and A. Chandra, "Control of single-phase solar photovoltaic supply system," *IEEE Transactions on Industry Applications*, vol. 56, no. 6, pp. 7132–7144, 2020.

[6] S. Shongwe and M. Hanif, "Comparative analysis of different single-diode PV modeling methods," *IEEE Journal of Photovoltaics*, vol. 5, no. 3, pp. 938–946, 2015.

[7] A. Sangwongwanich, Y. Yang, and F. Blaabjerg, "High-performance constant power generation in grid-connected PV systems," *IEEE Transactions on Power Electronics*, vol. 31, no. 3, pp. 1822–1825, 2016.
[8] R. Zhang, M. Cardinal, P. Szczesny, and M. Dame, "A grid simulator with control of single-phase power converters in D-Q S rotating frame," in *Proc. 33rd Annual IEEE Power Electronics Specialists Conference*, vol. 3, 2002, pp. 1431–1436.
[9] Y. Gu, N. Bottrell, and T. C. Green, "Reduced-order models for representing converters in power system studies," *IEEE Transactions on Power Electronics*, vol. 33, no. 4, pp. 3644–3654, 2018.
[10] "IEEE standard for interconnection and interoperability of distributed energy resources with associated electric power systems interfaces," *IEEE Std 1547-2018 (Revision of IEEE Std 1547-2003)*, pp. 1–138, 2018.

APPENDIX

TABLE I
SYSTEM PARAMETERS.

Technical Specifications			
$\boldsymbol{P_{nom}}$	$5kW$	$\boldsymbol{Q^{ref}}$	$0.5kVAr$
$\boldsymbol{I_{ph,STC}}$	$6.24A$	$\boldsymbol{V_{DC}^{ref}}$	$600V$
$\boldsymbol{I_{0,STC}}$	$2.18e-12A$	Grid voltage	$277Vrms$
$\boldsymbol{R_s}$	0.52Ω	$f_{SW}^{inv.}$	10 kHz
$\boldsymbol{R_{sh}}$	431Ω	f_{SW}^{boost}	20 kHz

TABLE II
VOLT-VAR AND VOLT-WATT DROOP SETTINGS [10].

Droop type	**Parameter**	**Value**
Volt-Var	V_N	277 (V)
	Q_{max}, V_1,V_2	2.2 (kVAr), $0.92V_N$, $0.98V_N$
	Q_{min}, V_3,V_4	-2.2 (kVAr), $1.02V_N$, $1.08V_N$
Volt-Watt	P_{max}, V_1	5 (kW), $1.06V_N$
	P_{min}, V_2	0, $1.1V_N$

TABLE III
EXECUTION TIME OF LVRT CASE STUDY FOR ALL MODELS.

Models	**Step size,** μs	**Execution time,** s
Detailed model	0.25	568.5
Average model	10	38
Simplified Average model	100	8
Phasor model	100	3.8